ACS OMEGA

http://pubs.acs.org/journal/acsodf

Article

New Thiazole Carboxamide Derivatives as COX Inhibitors: Design, Synthesis, Anticancer Screening, In Silico Molecular Docking, and ADME Profile Studies

Mohammed Hawash,* Nidal Jaradat,* Rozan Sabobeh, Murad Abualhasan, and Mohammed T. Qaoud

Cite This: *ACS Omega* 2023, 8, 29512−29526

Read Online

ACCESS | Metrics & More | Article Recommendations | Supporting Information

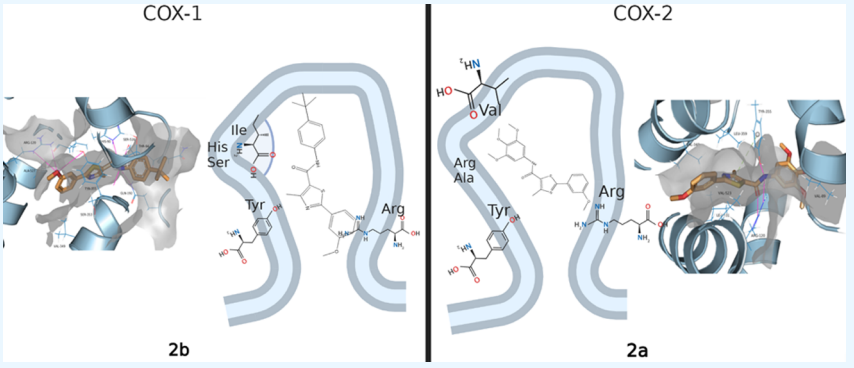

ABSTRACT: The goal of this work was to create and test a new series of thiazole carboxamide derivatives for their cyclooxygenase (COX) suppressor and anticancer effects. The compounds were characterized using 1H, 13C NMR, and HRMS spectrum analysis, and their selectivity toward COX-1 and COX-2 was assessed using an in vitro COX inhibition assay kit. Cytotoxicity was assessed using an MTS assay against a panel of cancer and normal cell lines. The docking studies were aided by the Prime MM-GBSA method for estimating binding affinities. The density functional theory (DFT) analysis was performed to assess compound chemical reactivity, which was calculated by computing the border orbital energy of both HOMO and LUMO orbitals, as well as the HOMO−LUMO energy gap. For ADME-T analysis, the QiKProp module was employed. Furthermore, using human X-ray crystal structures, molecular docking studies were carried out to discover the probable binding patterns of these drugs within both COX-1 and COX-2 isozymes. The results demonstrated that the most effective compound against the COX-1 enzyme was **2b** with an IC_{50} of 0.239 μM. It also showed potent activity against COX-2 with an IC_{50} value of 0.191 μM and a selectivity ratio of 1.251. The highest selectivity ratio was 2.766 for compound **2a** against COX-2 with an IC_{50} dose of 0.958 μM relating to the celecoxib ratio of 23.8 and its IC_{50} against COX-2 of 0.002 μM. Compound **2j** also showed good selectivity toward COX-2 (1.507) with an IC_{50} value of 0.957 μM. All compounds showed negligible cytotoxic activity against the evaluated normal cell lines, and the IC_{50} values were more than 300 μM, except for compound **2b**, whose IC_{50} values were 203.71 ± 1.89 and 116.96 ± 2.05 μM against LX-2 and Hek293t cell lines, respectively. Moreover, compound **2b** showed moderate anticancer activity against COLO205 and B16F1 cancer cell lines with IC_{50} values of 30.79 and 74.15 μM, respectively.

INTRODUCTION

Nonsteroidal anti-inflammatory drugs (NSAIDs) are a class of medicines that are usually used to treat inflammation, pain, and fever. They work by inhibiting the activity of the COX enzymes, which are responsible for the biosynthesis of prostaglandins, which are lipid mediators that play a main role in inflammatory responses. There are two main isoforms of COX enzymes, including COX-1 and COX-2; COX-1 is expressed constitutively in most tissues and is involved in maintaining normal physiological functions, such as platelet aggregation, gastric mucosal protection, and renal blood flow regulation, while COX-2 is encouraged in response to proinflammatory stimulants and is mainly responsible for the production of prostaglandins that mediate pain.[1−3]

NSAIDs can be classified into two main groups based on their selectivity for COX-1 and COX-2 enzymes. Nonselective NSAIDs, such as aspirin and ibuprofen, inhibit both COX-1 and COX-2 enzymes, while selective COX-2 inhibitors, such as

Received: May 10, 2023
Accepted: July 20, 2023
Published: August 6, 2023

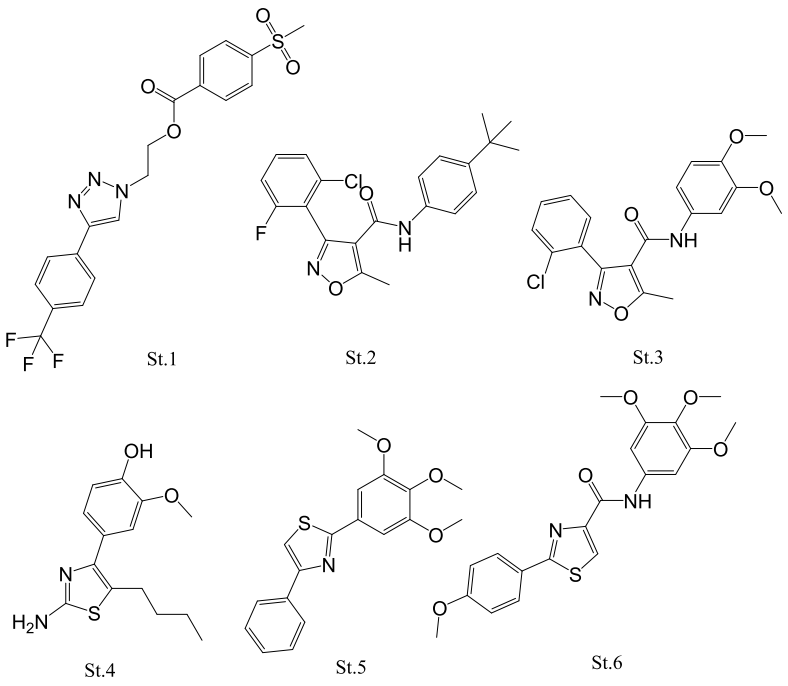

St.	IC_{50} (μM) of COX-1	IC_{50} (μM) of COX-2	SI
St.1	0.325	0.002	162.50
St.2	12.03	8.32	1.44
St.3	0.064	0.013	4.63
St.4	5.56 X 10^{-8}	9.01	<0.001
St.5	34.53	23.26	1.48
St.6	-	-	3.67

Figure 1. Chemical structures of COX inhibitors with heterocyclic rings including triazole (St.1), isoxazole (St.2 and St.3), and thiazole (St.4–St.6), with their IC_{50} values and selectivity ratios.

celecoxib, selectively inhibit the COX-2 enzyme.[4,5] Although NSAIDs are generally considered safe and effective, they can have adverse effects on the gastrointestinal tract, cardiovascular system, and renal function, especially with prolonged use or in high doses. Therefore, it is important to use NSAIDs judiciously and under the guidance of a healthcare professional.[6−8]

Both COX-1 and COX-2 enzymes have similar amino acid sequences, with roughly 67% of these amino acids being identical. The remaining amino acids differ, with COX-1 having isoleucine (ILE-523) instead of valine (VAL-523) in COX-2, resulting in a larger COX-2 binding pocket than a COX-1 binding pocket.[9] Long-term usage of COX-1 inhibitor drugs often results in GIT adverse effects like ulcers, as well as kidney or liver damage.[10] As a response, scientists attempted to develop selective NSAIDs like valdecoxib, celecoxib, and rofecoxib to alleviate the aforementioned side effects. However, the long-term use of these medicines reduces prostaglandin I2 production, resulting in cardiovascular adverse effects.[11] As a result, safer and more specific inhibitors must be developed. According to research, tricyclic derivatives showed superior COX-2/COX-1 ratios to standard NSAIDs such as aspirin and ketoprofen.[12]

Many heterocyclic-containing drugs, including pyrazole, tetrazole, isoxazole, and thiazole derivatives, have recently demonstrated COX inhibitory activity. The most selective molecule toward COX-2 in the produced triazole series was compound St.1 (Figure 1).[6] Previously, we sought to synthesize and test a variety of phenyl-heterocycle-carboxamides for COX inhibitory activity. At various places on the phenyl ring, electron-withdrawing elements such as F and Cl were replaced.[3,13] However, practically, all of these compounds were shown to be active against both COX-1 and COX-2, with selectivity toward COX-2, and compound St.2 (Figure 1) was the most selective one with a selectivity ratio of 1.44.[3] The selectivity increased with compound St.3 (Figure 1) when the ratio of carboxamide-phenyl-containing dimethoxy groups was 4.63.[13] Many thiazole-containing compounds were developed and tested as COX inhibitors with substantial activity.[14,15] A variety of aminothiazole derivatives were synthesized, and compound St.4 (Figure 1) demonstrated significant inhibitory activity with an IC_{50} value of 5.56×10^{-8} μM against COX-1, with a very low selectivity ratio to COX-2.[16] In another investigation, a series of 2-(trimethoxyphenyl)thiazole derivatives were synthesized, with compound St.5 (Figure 1) being one of the most powerful COX enzyme inhibitors.[17] In our last work regarding the thiazole carboxamide derivative, compound St.6 (Figure 1) had a selectivity ratio of 3.67 at 5 μM concentration and a bulky trimethoxy group on the phenyl ring that could not bind effectively with the COX-1 enzyme.[18]

The COX-2 enzyme is commonly overexpressed in a variety of human malignancies, and biological investigations have repeatedly demonstrated that COX-2 inhibitor drugs can decrease tumor progression and metastasis in a variety of animal cancer models. Moreover, several studies have shown that COX-2 inhibitors can work synergistically with currently used anticancer agents.[19] Furthermore, some research has suggested that COX inhibitors, particularly COX-2 inhibitors,

https://doi.org/10.1021/acsomega.3c03256
ACS Omega 2023, 8, 29512−29526

Scheme 1. After Stirring 1 + Aniline Derivatives in 20 mL of DCM, (a) DMAP and (b) EDC were Added under Argon Gas and Stirred for 48−72 h

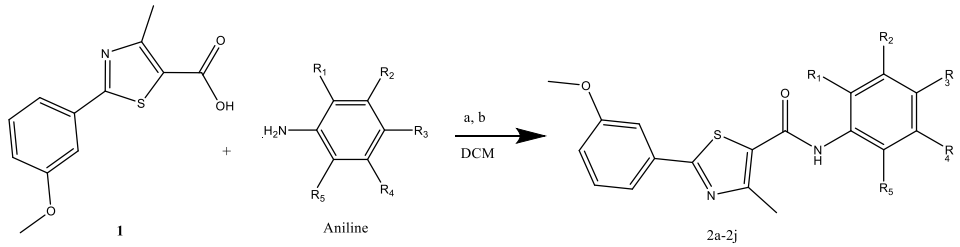

Compound	R1	R2	R3	R4	R5
2a	H	$-OCH_3$	$-OCH_3$	$-OCH_3$	H
2b	H	H	-t-butyl	H	H
2c	H	$-OCH_3$	$-OCH_3$	H	H
2d	H	$-OCH_3$	H	$-OCH_3$	H
2e	H	H	$-S-CH_3$	H	H
2f	H	H	H	H	H
2g	$-OCH_3$	H	$-OCH_3$	H	H
2h	$-OCH_3$	H	H	$-OCH_3$	H
2i	H	H	-O-Ph-2-OCH_3	H	H
2j	H	CF_3	H	H	H

Table 1. Half-Maximal Inhibitory Concentration (IC_{50}) and Selectivity Index (SI) for Thiazole Carboxamide Derivative Compounds

		IC_{50} (μM)			CC_{50} (μM)	
code	R	COX-1	COX-2	SI	Hek293t	LX-2
2a	3,4,5-triemthoxyphenyl	2.650 ± 0.78	0.958 ± 0.12	2.766	>300	>300
2b	4-*t*-butyl	0.239 ± 0.18	0.191 ± 0.05	1.251	116.963 ± 2.05	203.716 ± 1.05
2c	3,4-dimethoxy	0.278 ± 0.02	2.906 ± 1.08	0.095	>300	>300
2d	3,5-dimethoxy	1.574 ± 0.80	2.298 ± 0.25	0.685	>300	>300
2e	4-S-CH_3	1.531 ± 0.92	2.117 ± 1.48	0.723	>300	>300
2f	H	2.055 ± 1.21	3.258 ± 1.02	0.630	>300	>300
2g	2,4-dimethoxy	0.632 ± 0.28	1.803 ± 0.05	0.350	>300	>300
2h	2,5-dimethoxy	0.335 ± 0.19	1.228 ± 0.85	0.272	>300	>300
2i	4-(2-methoxyphenoxy)	2.111 ± 1.08	3.239 ± 1.11	0.651	>300	>300
2j	3-CF3	1.443 ± 0.51	0.957 ± 0.17	1.507	>300	>300
+Ve con		0.048 ± 0.02[a]	0.002 ± 0.001[a]	23.8[a]	4.058 ± 1.82[b]	8.45 ± 2.02[b]

[a]Note: *P*-value ≤ 0.05; positive controls: celecoxib. [b]5-FU.

may have antitumor effects and could be used as a cancer treatment.[20,21]

The current study seeks to generate a novel series of thiazole carboxamide derivatives (**2a−2j**) and analyze their activities on COX enzymes as well as their cytotoxicity on a panel of cancer and normal cell lines based on prior findings. That is a great approach to further validating the potential of our compounds as COX inhibitors. Molecular docking studies can provide insights into the binding interactions between the COX enzymes and our compounds, which can help explain their observed COX inhibition activity. By studying the binding patterns of the synthesized compounds within the binding domains of COX-1 and COX-2 enzymes, we can gain a better understanding of their selectivity and potential for therapeutic use. For example, if these compounds show a strong binding affinity for COX-2 but not for COX-1, they may be useful for treating inflammation without causing unwanted side effects associated with COX-1 inhibition, such as gastric ulcers. Moreover, the molecular dynamics simulations and density functional theory (DFT) calculations on these compounds can provide further insights into their structural stability, conformational flexibility, and electronic properties. Overall, the combination of in vitro assays and molecular docking studies can provide a comprehensive understanding of the potential of our compounds as COX inhibitors and can guide further development of these compounds as potential therapeutics.

RESULTS AND DISCUSSION

Chemistry. According to Scheme 1, thiazole carboxamide derivatives (**2a−2j**) were created. 2-(3-Methoxyphenyl)-4-

https://doi.org/10.1021/acsomega.3c03256
ACS Omega 2023, 8, 29512−29526

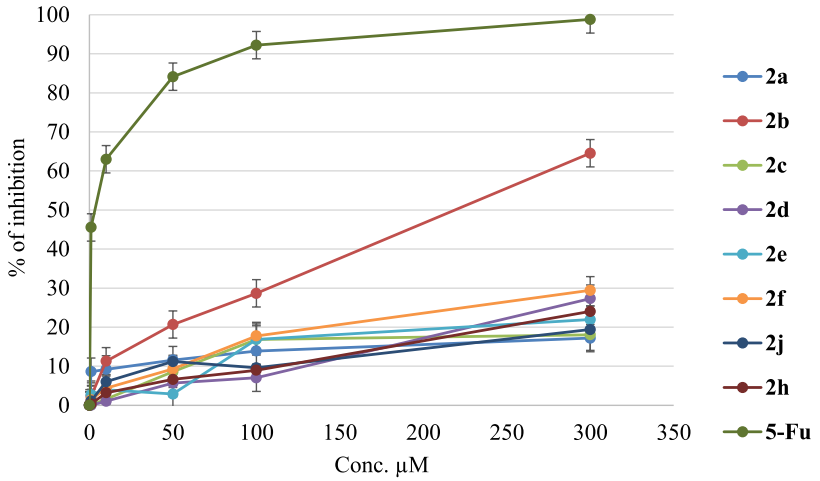

Figure 2. Inhibition percentage of all compounds compared to the positive control 5-FU by using LX-2 cells.

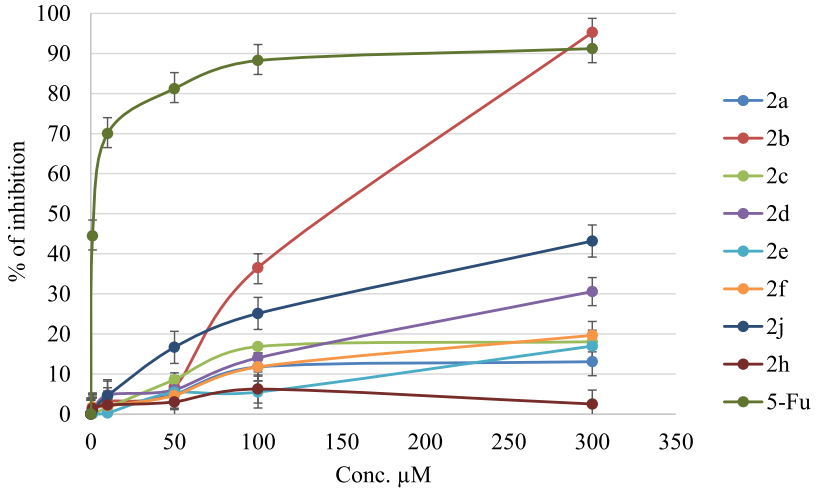

Figure 3. Inhibition percentage of all compounds compared to the positive control 5-FU by using Hek293t cells.

methylthiazole-5-carboxylic acid was dissolved in DCM, and then DMAP and EDCI were added and mixed under argon gas to create 2-(3-methoxyphenyl)-4-methyl-N-(3,4,5-trimethoxyphenyl)thiazole-5-carboxamide compound **2a**. 3,4,5-Trimethoxyaniline was added after 30 min, and the reaction was stirred for 48 h before being extracted with HCl 32% and sodium sulfate anhydrous, and filtration was done. Except for **2e**, **2f**, **2g**, **2h**, and **2j** compounds, most of the produced products were purified using column chromatography.

Biological Results. *In Vitro COX-1 and COX-2 Inhibition Assay.* All compounds were tested for inhibition on COX-1 and COX-2 enzymes using the Cayman Chemical Company's COX-1 (human) Inhibitor Screening Assay Kit and the COX-2 (human) Inhibitor Screening Assay Kit (Ann Arbor, MI). As demonstrated in Table 1, all synthesized compounds had considerable inhibitory activity at both COX enzymes at the utilized concentrations. From the IC_{50} values and selectivity ratios, we can see that compound **2a** is the most selective compound for COX-2 over COX-1, with a selectivity ratio of 2.76618. When the selectivity ratio is close to 1.0, the NSAID is typically classified as a nonselective COX inhibitor. Conversely, NSAIDs with selectivity ratios less than 1 are considered more selective for COX-1 inhibition.[22] On the other hand, NSAIDs with selectivity ratios greater than 1 are considered to be more potent in inhibiting COX-2. In our study, compound **2a** demonstrated a selectivity ratio greater than 1 (2.76), indicating a higher potency in inhibiting COX-2 than that in COX-1.

Compound **2b** is the most potent compound that exhibits the lowest IC_{50} values for both COX-1 and COX-2. Compound **2b**'s increased potency may be explained by the presence of a *t*-butyl substituent in comparison to the other compounds, which possess hydrophilic methoxy groups. The *t*-butyl group is a large lipophilic group that can interact with hydrophobic areas of the COX active site, perhaps resulting in greater binding and enzyme inhibition. The fact that compound **2b** has the lowest IC_{50} value for both COX-1 and COX-2 enzymes, suggesting increased potency, supports this. Moreover, compound **2b**'s *t*-butyl group may interact with the hydrophobic channel of the COX active site via van der Waals forces, hydrophobic contacts, and/or steric hindrance. This interaction could improve the compound's binding affinity to the COX enzyme, resulting in greater potency. The hydrophilic methoxy groups of the other chemicals, on the other hand, may interact with the hydrophilic channel of the COX active site via hydrogen bonding and/or electrostatic interactions. These interactions, however, may not be as strong as those

https://doi.org/10.1021/acsomega.3c03256
ACS Omega 2023, 8, 29512−29526

Table 2. Cytotoxicity of Target Compounds 2a−2j Indicated with Their IC_{50} (μM) Values in Seven Cancer Cell Lines[a]

	IC_{50} (μM)						
new code	Hep3B	HepG2	HeLa	MCF-7	COLO205	CaCo-2	B16F1
2a	>300	60.75 ± 2.76	>300	>300	>300	>300	>300
2b	>300	>300	>300	>300	30.79 ± 0.49	>300	74.15 ± 2.44
2c	>300	>300	>300	>300	>300	>300	>300
2d	>300	>300	>300	143.68 ± 2.03	>300	>300	>300
2e	202.11 ± 1.99	>300	222.97 ± 2.58	162.88 ± 2.88	>300	>300	>300
2f	>300	>300	>300	>300	>300	>300	>300
2g	>300	>300	>300	>300	>300	>300	>300
2h	>300	>300	250.80 ± 2.42	>300	>300	>300	>300
2i	>300	>300	>300	>300	>300	>300	>300
2j	299.17 ± 2.05	>300	>300	>300	>300	>300	>300

[a]Note: P-value ≤ 0.05.

between the *t*-butyl group and the hydrophobic channel, resulting in reduced efficacy. Comparing compound **2a** to the St.6 structure (Figure 1), it was observed that both compounds exhibited comparable selectivity against COX-1 and COX-2 enzymes. St.6 displayed a selectivity index of 3.67, while **2a** has a selectivity index of 2.76 for COX-2 over COX-1, indicating a higher preference for COX-2 inhibition in both cases. While St.6 displayed only moderate inhibition activity at 5 mM, with 53.9% inhibition of COX-2 and 14.7% inhibition of COX-1, compound **2a** exhibited enhanced potency with COX-2 IC_{50} = 0.95 μM and COX-1 IC_{50} = 2.65 μM. Although the selectivity of compound **2a** remains comparable to that of St.6, the structural modification introduced in compound **2a** has led to a notable improvement in inhibition potency against both COX isoforms. This modification has resulted in an overall increase in potency for compound **2a**. The enhanced potency is believed to be attributed to the unique scaffold of compound **2a** compared to St.6. In particular, the introduction of the methyl group at the thiazole position in our newly designed compounds has positively influenced the geometrical conformation of compound **2a**. This modification has improved the fitting geometry by altering the overall shape and conformation of the molecule. Furthermore, it is proposed that this structural modification may have influenced the orientation and spatial arrangement of the surrounding functional groups, potentially affecting the interactions with the COX active site and reducing steric clashes.

The fact that none of the compounds showed considerable cytotoxicity on normal cell lines (LX-2 and Hek293t) with CC_{50} values higher than 300 μM (Table 1) except for compound **2b** (CC_{50} values were 203.71 ± 1.89 and 116.96 ± 2.05 μM against LX-2 and Hek293t cell lines, respectively) is a promising sign for their potential as therapeutic candidates. The inhibition percentage of all of these compounds is presented in Figures 2 and 3 compared to the positive control 5-FU. The low toxicity of compound **2b**, on the other hand, could be due to the *tert*-butyl group, which improves its lipophilicity, which may contribute to enhanced cellular absorption and accumulation. This could result in increased intracellular quantities of the substance, which could result in cytotoxicity.

Anticancer Screening. All compounds were further investigated by the MTS assay on hepatocellular carcinoma (Hep3B and HepG2), cervical adenocarcinoma (HeLa), breast carcinoma (MCF-7), melanoma (B16F1), colorectal adenocarcinoma (Caco-2), and colon adenocarcinoma (COLO205), to evaluate their antiproliferative activities and find the relation between COX inhibitors and anticancer activities; almost all of these compounds showed negligible activities on the mentioned cancer cell lines with IC_{50} > 300 μM (Table 2) except for compound **2a** against HepG2 with an IC50 value of 60.75 μM and compound **2b** against COLO205 and B16F1 cancer cell lines with IC50 values of 30.79 and 74.15 μM, respectively.

Compound **2a**'s increased action against HepG2 cancer cell lines may be related to its capacity to selectively inhibit COX enzymes, which have been demonstrated to be overexpressed in many cancer cell types, including HepG2 cells. Over the past decade, numerous structures based on trimethoxyphenyl have been designed, developed, and synthesized as potential anticancer agents with the ability to specifically target the tubulin protein,[23,24] and some of these compounds reached clinical trials or were approved by FDA for cancer treatment.[25−27] The trimethoxyphenyl group, which is one of the main parts of compound **2a**, was present in many potent anticancer agents like combretastatin A-4 (CA-4); this moiety in CA-4 is believed to contribute to its biological activity by enhancing the compound's lipophilicity and membrane permeability. In addition, the three methoxy groups can form hydrogen bonds with the target protein, potentially increasing the compound's binding affinity and selectivity.[28] Additionally, compound **2a** may have other mechanisms of action that contribute to its antiproliferative activity in HepG2 cells. Compound **2b**'s cytotoxicity on COLO205 and B16F1 cancer cell lines could be attributed to the lipophilic character of the *tert*-butyl group. Lipophilic substances are more membrane-permeable, which may result in greater cellular absorption and interaction with intracellular targets such as COX enzymes.

Molecular Docking Studies. To investigate the pattern of ligand−protein binding and orientations within the binding site of COX-1 and COX-2 isozymes, so explaining the COX-2 selectivity over the COX-1 recorded for celecoxib, A, B, and J-molecules, molecular docking studies have been performed. However, the amino acid sequence identity of both isoforms is equal to 67%, replacing the ILE-523 amino acid accommodated inside the binding site of COX-1 with the amino acid VAL-523 in COX-2, resulted in the opening of a new secondary binding pocket. This led to uncovering of the new polar amino acid ARG-513, which could involve many polar interactions within the binding site of COX-2. Thus, interacting with ARG-513 is considered an ameliorating COX-2 selectivity.

For each ligand, 30 different orientations were retained from docking simulations. The orientation of each ligand, which

https://doi.org/10.1021/acsomega.3c03256
ACS Omega 2023, 8, 29512−29526

revealed the lowest binding Glide docking score within the enzyme's binding pocket, was selected as the best to be discussed. Table 3 summarizes all docking scores of the docked ligands inside COX-1 and COX-2 enzymes. The docking simulations of celecoxib, **2a**, **2b**, and **2j** molecules inside COX-1 and COX-2's enzyme binding location are shown in Figures 4 and 5. Examining the binding pattern of celecoxib as an ideal COX-2 selective (selectivity index (SI) = 23.8) drug over COX-1 showed the optimal occupying and interaction pattern within the COX-2 binding site (Figure 5a), which involves filling the newly generated secondary binding pocking and interacting with ARG-513, which are critical interactions for COX-2 selectivity. This additional occupied space and interactions diminished IC_{50} from 47 nM in COX-1 to just 2 nM in COX-2. The absence of this secondary binding pocket in COX-1 (Figure 4a) results in rotating the sulfonamide group toward SER-516. Thus, the 4-methylphenyl group generates some steric clashes with the larger amino acid ILE-523 inside COX-1 than VAL-523 presents in COX-2. Other favorable interactions like hydrogen bonds, hydrophobic interactions, and pi−cation interactions also support the significant inhibition activity of celecoxib in the COX-2 enzyme.

Table 3. Docking Scores of the Newly Designed Ligands within the COX-1 and COX-2 Receptors and the Free Energy Calculation (ΔG_{bind}) of Ligand−Drug Complexes Using Prime/MM-GBSA

	COX-1		COX-2	
ligands	docking score	ΔG_{bind}	docking score	ΔG_{bind}
2a	−5.59	−50.75	−5.93	−58.07
2b	−5.60	−43.39	−8.39	−70.72
2j	−6.09	−58.33	−6.93	−62.94
celecoxib	−10.86	−73.89	−11.28	−80.18

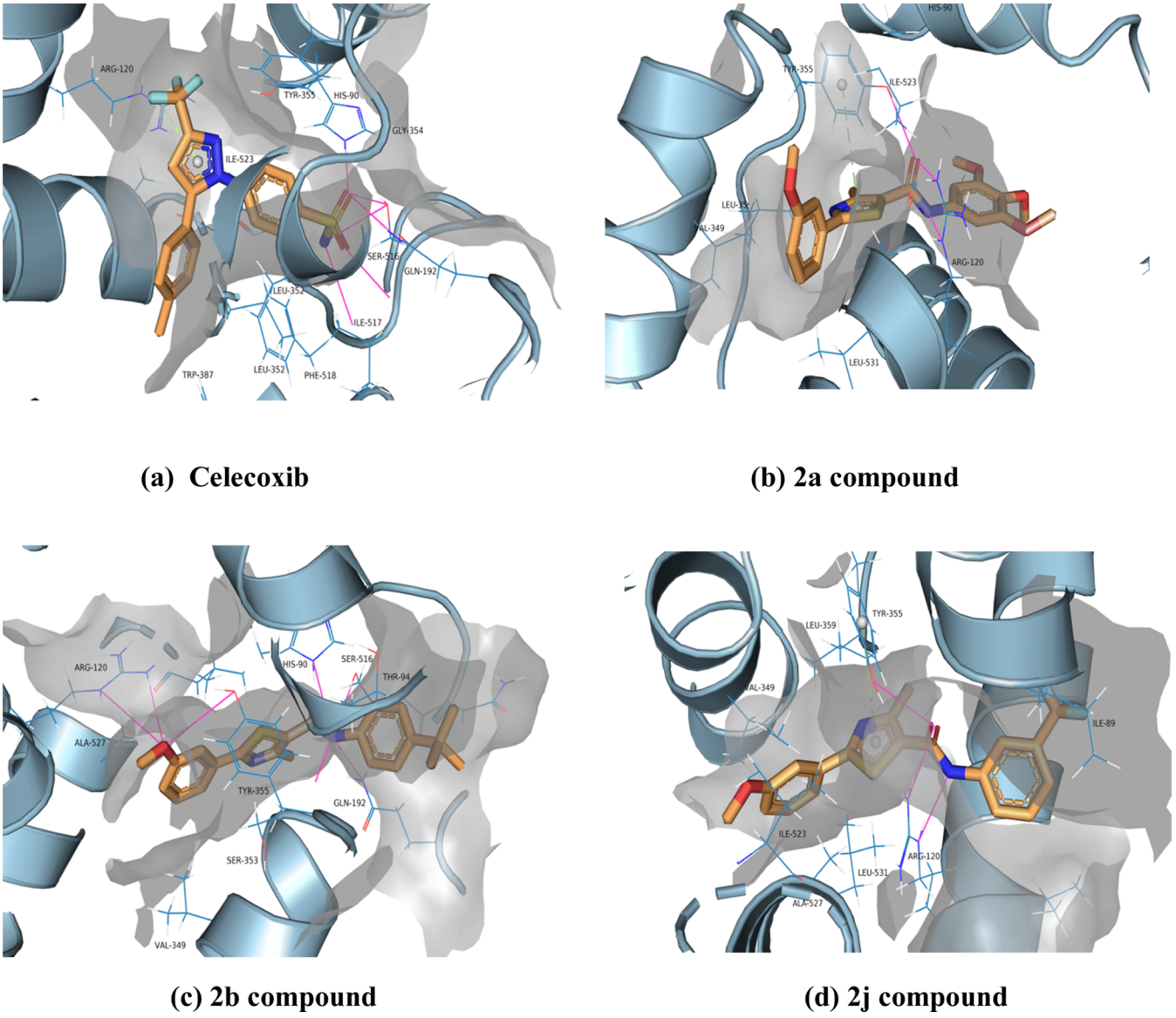

Figure 4. Docking simulation of celecoxib (a), **2a** (b), **2b** (c), and **2j** (d) molecules across the binding location of COX-1 (PDB ID: 3KK6). A 3D gray surface is used to represent the active site (transparency 50%). Ligands are shown as stick structures—orange color. Light magenta lines represent hydrogen bonds; light green dashed lines indicate the presence of the Pi−cation bond.

https://doi.org/10.1021/acsomega.3c03256
ACS Omega 2023, 8, 29512−29526

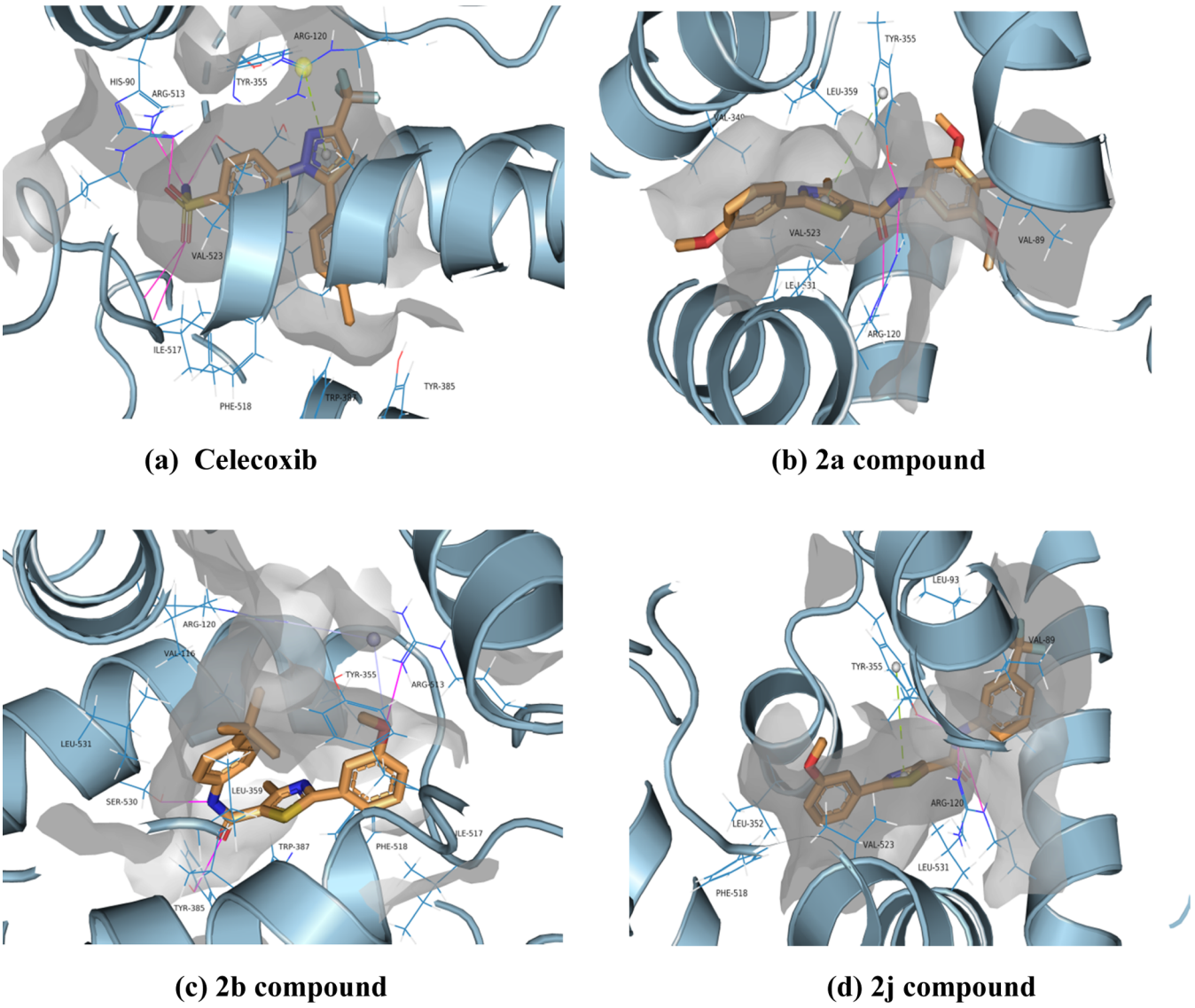

Figure 5. Docking simulation of celecoxib (a), **2a** (b), **2b** (c), and **2j** (d) molecules in COX-2 (PDB ID: 5KIR). A 3D gray surface is used to represent the active site (transparency 50%). Ligands are shown as stick structures—orange color. Light magenta lines represent hydrogen bonds; light green dashed lines indicate the presence of the Pi−cation bond.

Examining the interaction and docking simulation pattern of the **2b** molecule, which displayed the most COX-2 inhibition activity (IC_{50} = 0.19 μM) in comparison to other newly designed molecules, showed its capability to fill the COX-2 binding site optimally, encompassing the available secondary polar binding pocket. A large substituent like a *t*-butyl group pushed the meta-methoxyphenyl fragment to step inside this secondary binding pocket, forming a critical and ameliorating hydrogen bond with ARG-513. Analyzing the docking simulation of **2b** using PLIP software indicated the formation of additional hydrogen bonds with TYR-385 and SER-530 and 13 water-repellent interactions between the nearby amino acids like VAL-116, PHE-518, ILE-517, and LEU-531 (Figure 5c). The high inhibition activity of the **2b** molecule recorded against the COX-1 isozyme (IC_{50} = 0.239 μM) could be explained by forming six favorable hydrogen bonds with TYR-355, HIS-90, ARG-120, GLN-192, SER-353, and SER-516 (Figure 4c). Also, the *t*-butyl group serves a crucial function in stabilizing the **2b** molecule in a good geometry within the COX-1 binding pocket by filling the available lipophilic space and forming hydrophobic interactions with the close amino acids like THR-94.

In the molecular docking studies of the **2a** molecule in Figures 4b and 5b, the binding sites for COX-1 and COX-2, respectively, are shown. The extended conformation of the **2a** molecule and 4,5,6-trimethoxy substituents show low congruency with the dimensions of the COX-1 binding site. Thus, the three methoxy substituents do not locate within the binding distances, so pay steric and electronic penalties to decrease the COX-1 inhibition potency (IC_{50} = 2.65 μM). **2a** molecule shows similar interaction patterns within the binding site of COX-2 (creates hydrogen bonds with ARG-120, TYR-355, and Pi−cation bond with TYR-355), but the 3,4,5-trimethoxy residue dips more in the binding pocket, resulting in forming more hydrophobic interactions with lipophilic residues like VAL-89, VAL-523, and LEU-359.

Replacing 3,4,5-trimethoxy in the **2a** molecule with −CF3 in the **2j** molecule led to enhancing COX-1 inhibition potency by 1 μM and keeping the COX-2 inhibition potency around 0.9 μM. As shown in Figures 4d and 5d, docking studies revealed

https://doi.org/10.1021/acsomega.3c03256
ACS Omega 2023, 8, 29512−29526

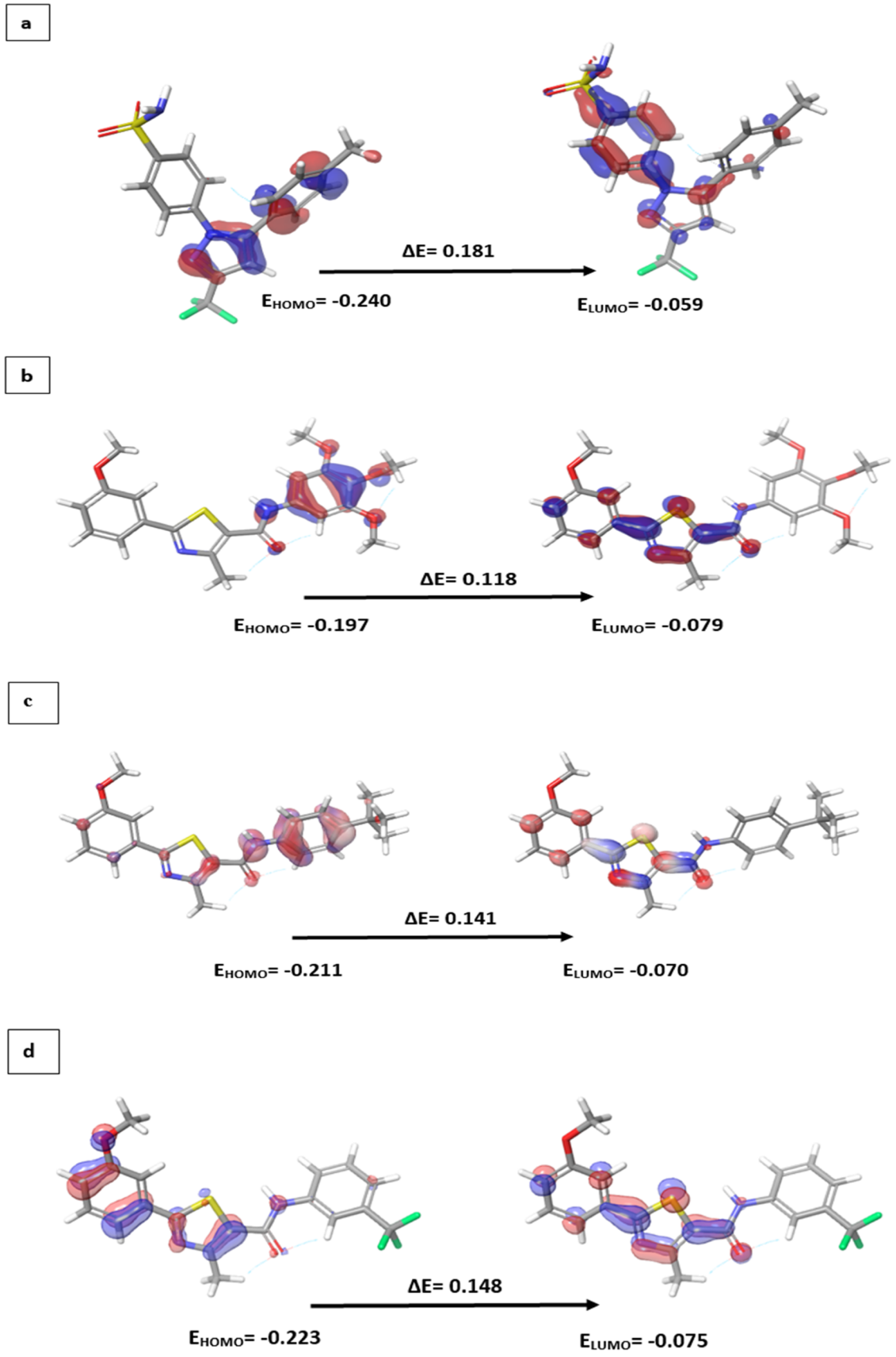

Figure 6. Celecoxib (a), **2a** (b), **2b** (c), and **2j** (d) molecules′ 3D highest occupied molecular orbital (HOMO), lowest unoccupied molecular orbital (LUMO), orbital energy values, and HOMO−LUMO energy gaps (*E*).

https://doi.org/10.1021/acsomega.3c03256
ACS Omega 2023, 8, 29512−29526

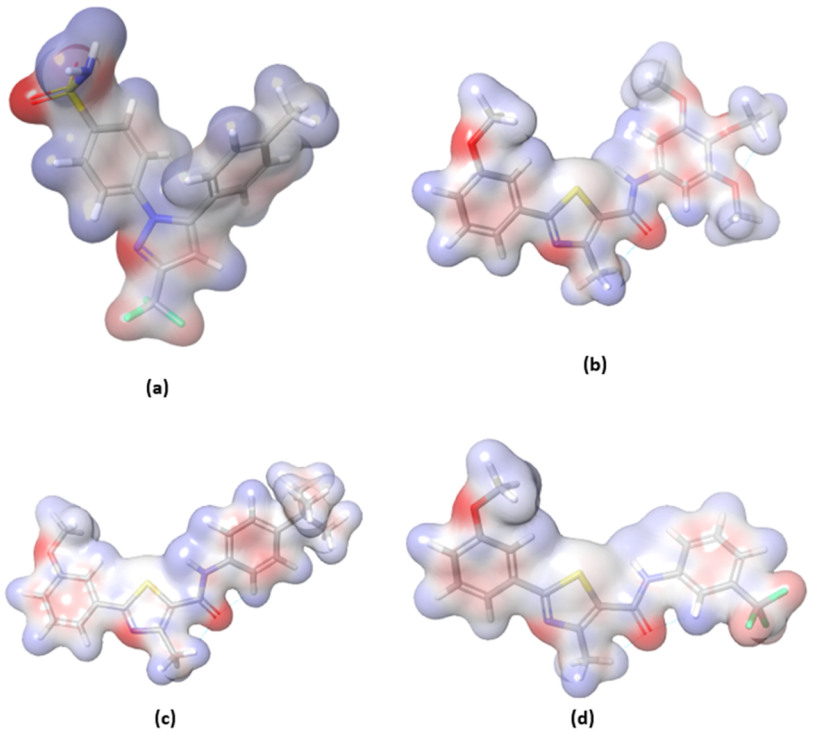

Figure 7. Electrostatic potential profiles of celecoxib (a), A (b), B (c), and J (d) molecules.

that the −CF3 group involves more in the COX-1 binding pocket than the trimethoxy group, so lesser electronic and steric clashes resulted in increasing the potency. The similar interaction pattern of the **2j** and **2a** molecules inside the COX-2 binding site is reflected by similar potency.

Prime MM/GBSA Analysis. To investigate the relative binding affinity of the positive control drug (celecoxib) and the three selected ligands (**2a**, **2b**, and **2j**) to COX-1 and COX-2 isozymes, MM/GBSA calculations were performed. Within the binding site of the COX-1 isozyme, celecoxib and the three selected molecules showed good binding free energy values (ΔG_{bind}) of −73.89, −50.75, −43.39, and −58.33 Kcal/mol, respectively. Making a binding free energy calculation of ligands within the COX-2 binding site resulted in ΔG_{bind} values of −80.18, −58.07, −70.72, and −62.94 kcal/mol for celecoxib, **2a**, **2b**, and **2j**, respectively. All of the MM-GBSA calculations are summarized in Table 3. As the calculated binding affinity (ΔG_{bind}) of celecoxib is lower than those of our tested molecules, celecoxib has a stronger affinity to both COX-1 and COX-2 active sites, which is consistent with the recorded XP Glide docking scores and biological results.

Density Functional Theory Analysis. The frontier orbital theory states that a molecule's stability and reactivity at the receptor binding site (ligand−receptor interactions) or in a chemical reaction could be precisely predicted based on certain features like the symmetries and shapes of HOMO and LUMO orbitals, which are mostly antibonding-type orbitals.[29] As shown in Figure 6, the highest occupied molecular orbital (HOMO) energy, the lowest unoccupied molecular orbital (ELUMO) energy, and the HOMO−LUMO energy gap (ΔE) were calculated besides visualizing the HOMO and LUMO maps for the reference drug (celecoxib) and **2a**, **2b**, and **2j** molecules. Positive lobes are shown by the color red, while the blue color designates negative lobes. These calculated electronic parameters were validated by observing the celecoxib electrostatic potential patterns and selected ligands, as shown in Figure 7. HOMO indicates the ability to donate electrons, while LUMO represents the capacity to take electrons. The HOMO−LUMO gap (ΔE) refers to the energy differential between HOMO and LUMO, which determines the optical polarizability, chemical reactivity, kinetic stability, and chemical hardness−softness.[30,31] Examining the HOMO maps indicates that the electron donor para-methyldiazole ring, 3,4,5-trimethoxyphenyl, *t*-butylphenyl, and 4-methoxyphenylthiazole fragments showed the highest electron density.

Hydrophobic interactions are favored for the phenyl rings of the high electron density HOMO fragments. Within the protein binding site, the impact of HOMO energy could be rationalized in terms of many valuable interactions like π---π and π---σ stacking and charge transfer between aromatic rings of molecules and residues at binding sites, while examining the LUMO profiles indicates that fragments of lower electron density locate over the sulfonamide phenyl of celecoxib and the thiazole-4-methoxyphenyl fragment of **2a**, **2b**, and **2j** molecules, suggesting the susceptibility of these parts toward nucleophilic attack.

As summarized in Figure 6, calculated HOMO energy values for celecoxib, **2a**, **2b**, and **2j** molecules are −0.240, −0.197, −0.211, and −0.223 eV, respectively. Similarly, the LUMO energy values are −0.059, −0.079, −0.070, and −0.075 eV. The tested ligands' chemical stability and reactivity could be predicted by calculating the HOMO−LUMO gap (ΔE), and the calculated ΔE values of celecoxib, **2a**, **2b**, and **2j** molecules are 0.181, 0.118, 0.141, and 0.148 eV, respectively. Higher energy gaps indicate higher chemical hardness and lower polarizability more energy is required for excitement from HOMO to LUMO.[32]

As shown in Figure 7, the electrostatic potential (ESP) map highlights the regions of negative potential around the oxygen atoms of carbonyl and methoxy groups within **2a**, **2b**, and **2j**

https://doi.org/10.1021/acsomega.3c03256
ACS Omega 2023, 8, 29512−29526

Table 4. ADME-T Characteristics of Synthetic Compounds Utilizing the Usual Mode of the QiKProp Module from Schrödinger 12.1, LLC, New York

		compounds										recommended values
		2a	2b	2c	2d	2e	2f	2g	2h	2i	2j	
ADME-T parameters	**Mol_MW**	414.4	380.5	384.4	384.4	370.4	324.3	384.4	384.4	446.5	392.3	130−725
	PSA	76.1	52.7	68.5	69.1	52.7	52.7	68.1	67.9	67.2	52.7	7−200
	SASA	726.8	713.3	688.2	686.3	675.9	612.7	690.8	689.6	784.9	664.3	300.0−1000.0
	FOSA	440.4	366.4	358.9	357.7	361.8	174.3	356.7	356.9	263.3	175.1	0.0−750.0
	FISA	44.8	46.5	44.6	44.8	46.8	46.6	48.3	46.1	45.9	46.6	7.0−330.0
	PISA	213.0	271.8	255.9	255.2	297.1	363.4	260.8	261.7	446.1	296.9	0.0−450.0
	WPSA	28.5	28.6	28.6	28.4	70.1	28.3	24.9	24.7	29.5	145.6	0.0−175.0
	volume	1280.9	1259.1	1195.4	1195.3	1163.6	1044.3	1204.7	1203.7	1388.3	1142.5	500.0−2000.0
	QPpolrz	43.2	44.2	40.9	40.9	40.6	37.1	41.3	41.3	49.8	40.4	13.0−70.0
	QPPCaco	3721	3586	3733	3717	3564	3580	3446	3618	3633	3579	<25 poor >500 great
	percent human oral absorption	100	100	100	100	100	100	100	100	100	100	>80% is high <25% is low
	#metab**	6	3	5	6	3	4	5	6	4	3	1−8
	dipole	5.66	4.82	5.64	5.61	3.89	4.90	6.87	5.06	7.72	6.58	1.0−12.5
	QPlogPo/w	4.48	5.29	4.25	4.25	4.64	4.05	4.27	4.28	5.78	5.03	−2.0 to 6.5
	QPlogPoct++	19.38	18.6	18.2	18.2	17.7	16.4	18.6	18.3	21.7	18.2	8.0−35
	QPlogBB	−0.21	−0.10	−0.14	−0.14	−0.01	−0.02	−0.19	−0.16	−0.24	0.24	−3 to 1.2
	QPlogHERG	−6.03	−6.02	−6.12	−6.08	−6.32	−6.30	−6.13	−6.12	−7.43	−6.25	below −5
	QPlogS	−6.03	−6.98	−5.80	−5.77	−6.05	−5.35	−5.83	−5.81	−7.46	−6.77	−6.0 to 0.5
	QPlogKhsa	0.44	0.93	0.41	0.41	0.57	0.40	0.43	0.43	0.93	0.66	−1.5 to 1.5
	rule of three	1	1	1	1	1	0	1	1	1	1	<3
	rule of five	0	1	0	0	0	0	0	0	1	1	<4

molecules and of the sulfone group within celecoxib. Also, the locations with low potential surrounding the nitrogen atoms within the diazole and thiazole rings of celecoxib and our tested ligands were highlighted, respectively. Inspecting the ESP profiles has many beneficial revenues because it influences the interactions between ligands and proteins at an early stage and allows the prediction of the critical sites for optimal binding.[33]

ADME-T Analysis. Estimating the ADME-T features of the newly developed drugs is a decisive indicator for successful development during the advanced stages of drug processing. Exhibiting unfavorable ADME-T parameters is often a stumbling block in advancing drug progression, which could ultimately lead to its elimination. Thus, our newly 10 designed ligands had been subjected to the QikProp module (Schrödinger 12.1, LLC, NY), and most incorporated physicochemical and pharmacokinetic parameters (ADME-T calculations) like molecular weight (Mol Mw), accessible surface area for solvents (SASA), polar surface area (PSA), hydrophilic component of the SASA (FISA), hydrophobic component of the SASA (FOSA), total solvent-accessible volume (Volume), π component of the SASA (PISA), predicted polarizability (QPpolrz), SASA component that is weakly polar (WPSA), predicted human oral absorption, predicted Caco-2 cell permeability (QPPCaco), computed dipole moment (Dipole), number of probable metabolic processes (#metab**), octanol/gas partition coefficient (QPlogPoct++), octanol/water partition coefficient (QPlogPo/w), brain/blood partition coefficient (QPlogBB), aqueous solubility (QPlogS), predicted blockage of HERG K+ channels (QPlogHERG), binding to human serum albumin (QPlogKhsa), number of violations of Jorgensen's rule of 3, and number of violations of Lipinski rule of 5 were investigated. All of the obtained calculations and the recommended values are listed in Table 4.

Based on ADME-T properties recorded for the tested molecules, all ligands showed optimal pharmacokinetic and physicochemical values within the desirable ranges. However, the predicted aqueous solubility of **2b**, **2i**, and **2j** molecules was slightly lower than the recommended value. As the other investigated parameters are located in the optimal desirable ranges, like the recorded 100% human oral absorption, this minor deviation could be bypassed and compensated. Thus, our newly discovered ligands are suitable for further development as anti-inflammatory drugs based on their observed potential drug-like properties and low toxicity.

CONCLUSIONS

The thiazole-based derivatives evaluated in this work showed potential COX inhibitory efficacy with varying selectivity ratios. Compound **2b**, which had a *tert*-butylphenyl substituent, demonstrated the most effective activity against both COX-1 and COX-2 enzymes while exhibiting little cytotoxicity against normal cells. Compound **2a** demonstrated a high selectivity ratio for the COX-2 enzyme and moderate cytotoxicity against the majority of cancer cell lines examined, except for HepG2 cells, which showed moderate activity. The presence of trimethoxyphenyl substituents in some of these compounds has previously been documented in compounds with anticancer activity, indicating their potential. According to the findings from molecular docking studies, the bulky *t*-butyl group in compound **2b** plays a crucial role in pushing the meta-methoxyphenyl fragment to optimize its accommodation within the secondary binding pocket. This conformational arrangement facilitates the formation of a critical hydrogen bond with ARG-513, resulting in an important interaction. To

https://doi.org/10.1021/acsomega.3c03256
ACS Omega 2023, 8, 29512−29526

enhance selectivity and improve inhibition potency against the COX-2 isoform, further modifications at the meta-methoxy moiety are proposed. Specifically, the introduction of specific functional groups or substituents at different positions could enhance affinity for COX-2 and strengthen the hydrogen bond interaction with ARG-513. Additionally, considering the significance of the ARG-513 residue, replacing the neutral methoxy group with a negatively charged substituent, such as acetic acid or its bioisosteric moieties, may facilitate the formation of salt−bridge interactions with the positively charged ARG-513 residue, resulting in further enhancing COX-2 affinity. By strategically designing compounds that optimize these interactions, it is proposed to increase potency against COX-2 while maintaining or improving selectivity over COX-1. These findings indicate that these compounds have the potential to be selective COX inhibitors, and they provide a promising starting point for further optimization and development of novel anticancer agents.

MATERIALS AND METHODS

Chemistry. All chemicals were bought from Sigma-Aldrich and Alfa Aesar chemical companies and used without additional purification. 2-(3-Methoxyphenyl)-4-methylthiazole-5-carboxylic acid (catalog # H54566), 1-(3-dimethylaminopropyl)-3-ethylcarbodiimide hydrochloride (EDC, catalog # A10807), 4-methylthioaniline (catalog # L04950), 4-(2-methoxyphenoxy)aniline (catalog # H32565), and 3-(trifluoromethyl)aniline (catalog # A15910) were bought from Alfa Aesar Company. 4-(Dimethylamino)pyridine (DMAP, catalog # 39405-50G), 3,4,5-trimethoxyaniline (catalog # T68209-10G), sodium sulfate anhydrous, silica gel (catalog # S74874), 4-*tert*-butylaniline (catalog # 209864), 3,4-dimethoxyaniline (catalog # A83008), 3,5-dimethoxyaniline (catalog # D130001), aniline (catalog # 132934), 2,4-dimethoxyaniline (catalog # D129801-100G), and 2,5-dimethoxyaniline (catalog # 112984-250G) were bought from Sigma-Aldrich Company. HCl 32%, COX inhibitor screening assay kit No. 560131 (Cayman Chemical), RPMI 1640 media[-](L-glutamine), DMEM media, Trypsin EDTA solution B, and MTS reagent were also used. L-Glutamine solution and fetal bovine serum, Brazil origin, both were bought from Sigma-Aldrich Company.

Melting points were defined with a Gallenkamp melting point apparatus, a Vacuubrand rotary evaporator complet, an Upland UV lamp, a LABOMED inverted fluorescence microscope, an ESCO laminar flow cabinet, a BIOBASE medical CO_2 incubator, a Lab Tech Digital water bath, a J.P. SELECTA digital vortex, and an ADAM balance.

To carry out ^{1}H NMR and ^{13}C NMR spectra, a Burker 500 MHz-Avance III High-Performance Digital FT-NMR spectrometer instrument was utilized, at the Faculty of Science, University of Jordan, Jordan. The solvent utilized in both instruments was DMSO-d_6, and the internal standard was tetramethylsilane. All chemical shifts were recorded as δ (ppm). High-resolution mass spectra data (HRMS) were collected using a water LCT Premier XE Mass spectrometer using the ESI (+) method at Pharmacy Faculty Gazi University Ankara-Turkey. COX inhibitor screening assay kit No. 560131 (Cayman Chemical) was used to determine the inhibitory activity of ovine COX-1 and the human recombinant COX-2 enzyme. Utilizing a UV spectrophotometer at a 415nm wavelength and a microplate reader (Bio-Rad Japan), the yellow result of this enzymatic reaction was identified.

General Procedure for the Synthesis of Thiazole Carboxamide (2a−2j). In a clean round-bottom flask, 2-(3-methoxyphenyl)-4-methylthiazole-5-carboxylic acid (300 mg, 1.203 mmol) was dissolved in 15 mL of DCM, and then DMAP (45mg, 0.361 mmol) was added and stirred under argon gas to prevent oxidation. After 5−10 min, EDCI (305.91 mg, 1.5639 mmol) was added, which is a coupling reagent, and stirred under argon gas; then, after 30 min, the aniline derivative was added, and the reaction mixture was stirred with a stirrer for 48 h. TLC papers were pigmented with ninhydrin to detect the presence of aniline. The other one was pigmented with bromocresol to detect the presence of acid, to be sure the product was pure. Then, the reaction mixture was washed with diluted HCl to separate the aniline derivative by a separatory funnel (extraction). The lower layer was leaked inside a conical flask. Sodium sulfate anhydrous (drying agent) was added to the flask and filtered by filter paper (filtration step). Silica gel was added (3−4 spatulas) to the filtrate, and then, vacuum evaporation was used to remove the reaction mixture by a rotary vacuum evaporator considering the DCM boiling point of 39.6 °C to have a product-loaded silica in the flask. The product-loaded silica was purified by silica gel column chromatography using a DCM/ethyl acetate (1:1) solvent system, and tubes containing the product were collected and then evaporated.[34−36]

*2-(3-Methoxyphenyl)-4-methyl-N-(3,4,5-trimethoxyphenyl)thiazole-5-carboxamide (**2a**).* A white powder product with R_f = 0.71 (DCM/EtOAc 1:1). The percentage yield was 66%. HRMS (m/z): $[M + H]^+$ calcd for $C_{21}H_{22}N_2O_5S$ 415.1240, found 415.1252. ^{1}H NMR (DMSO-d_6, 500 MHz) δ ppm: 10.16 (1H, s, N−H), 7.55 (1H, d, J = 7.5 Hz, Ar−H), 7.49−7.12 (5H, m, Ar−H), 3.86 (3H, s, O−CH_3), 3.77 (6H, s, O−CH_3), 3.65 (3H, s, O−CH_3), 2.66 (3H, s, −CH_3). ^{13}C NMR (DMSO-d_6, 125 MHz) δ ppm: 166.4, 160.2, 160.0, 156.4, 153.1 (2C), 135.2, 134.5, 134.1, 131.1, 126.5, 119.2, 117.5, 111.3, 98.6 (2C), 60.6, 56.2 (2C), 55.8, 17.6.

*Synthesis of N-(4-(tert-Butyl) phenyl)-2-(3-methoxyphenyl)-4-methylthiazole-5-carboxamide (**2b**).* A beige crystal product with R_f = 0.6 (Hex/EtOAc 3:2). The percentage yield is 50%. HRMS (m/z): $[M + H]^+$ calcd for $C_{22}H_{24}N_2O_2S$ 383.1320, found 383.1313. ^{1}H NMR (DMSO-d_6, 500 MHz) δ ppm: 10.20 (1H, s, N−H), 7.61 (2H, d, J = 7 Hz, Ar−H), 7.55 (1H, d, J = 7.5 Hz, Ar−H), 7.49 (1H, s, Ar−H), 7.46 (1H, t, J = 8 Hz, Ar−H), 7.38 (2H, d, J = 7 Hz, Ar−H), 7.12 (1H, d, J = 8 Hz, Ar−H), 3.86 (3H, s, O−CH_3), 2.66 (3H, s, −CH_3), 1.29 (9H, s, *t*-butyl). ^{13}C NMR (DMSO-d_6, 125 MHz) δ ppm: 166.4, 160.2, 160.1, 155.9, 146.9, 136.5, 134.1, 131.1, 126.9, 125.8 (2C), 120.6 (2C), 119.2, 117.5, 111.3, 55.8, 34.6, 31.6 (3C), 17.6.

*N-(3,4-Dimethoxyphenyl)-2-(3-methoxyphenyl)-4-methylthiazole-5-carboxamide (**2c**).* A soft gray powder product with R_f = 0.74 (DCM/EtOAc 1:1). The percentage yield is 44%. HRMS (m/z): $[M + H]^+$ calcd for $C_{20}H_{20}N_2O_4S$, 385.1085, found 385.1099. ^{1}H NMR (DMSO-d_6, 500 MHz) δ ppm: 10.10 (1H, s, N−H), 7.55 (1H, d, J = 7.5 Hz, Ar−H), 7.49−7.44 (2H, m, Ar−H), 7.38 (1H, s, Ar−H), 7.25 (1H, d, J = 8.5 Hz, Ar−H), 7.12 (1H, d, J = 8 Hz, Ar−H), 6.94 (1H, d, J = 8.5 Hz, Ar−H), 3.86 (3H, s, O−CH_3), 3.76, 3.75 (6H, s, OCH3), 2.66 (3H, s, −CH_3). ^{13}C NMR (DMSO-d_6, 125 MHz) δ ppm: 166.3, 160.2, 159.8, 156.0, 148.9, 145.9, 134.1, 132.5, 131.1, 126.8, 119.2, 117.4, 112.9, 112.3, 111.3, 105.9, 56.2, 55.9, 55.8, 17.6.

https://doi.org/10.1021/acsomega.3c03256
ACS Omega 2023, 8, 29512−29526

*N-(3,5-Dimethoxyphenyl)-2-(3-methoxyphenyl)-4-methylthiazole-5-carboxamide (**2d**).* A white crystal product with R_f = 0.74 (DCM/EtOAc 1:1). The percentage yield is 56%. HRMS (m/z): $[M + H]^+$ calcd for $C_{20}H_{20}N_2O_4S$, 385.1085, found 385.0765. ^{1}H NMR (DMSO-d_6, 500 MHz) δ ppm: 10.19 (1H, s, N−H), 7.55 (1H, d, J = 7.5 Hz, Ar−H), 7.49−7.44 (2H, m, Ar−H), 7.12 (1H, d, J = 7.5 Hz, Ar−H), 6.99 (2H, s, Ar−H), 6.30 (1H, s, Ar−H), 3.86 (3H, s, O−CH_3), 3.74 (6H, s, OCH3), 2.65 (3H, s, −CH_3). ^{13}C NMR (DMSO-d_6, 125 MHz) δ ppm: 166.5, 160.9 (2C), 160.2 (2C), 156.3, 140.8, 134.1, 131.1, 126.6, 119.2, 117.5, 111.3, 98.9 (2C), 96.5, 55.8, 55.6 (2C), 17.61.

*2-(3-Methoxyphenyl)-4-methyl-N-(4-(methylthio)phenyl)-thiazole-5-carboxamide (**2e**).* A coarse dark green powder product with R_f = 0.75 (DCM/EtOAc 1:1). The percentage yield is 65.5%. HRMS (m/z): $[M + H]^+$ calcd for $C_{19}H_{18}N_2O_2S_2$, 371.0515, found 371.0508. ^{1}H NMR (DMSO-d_6, 500 MHz) δ ppm: 10.29 (1H, s, N−H), 7.67 (2H, d, J = 8 Hz, Ar−H), 7.55 (1H, d, J = 7.5 Hz, Ar−H), 7.49−7.44 (2H, m, Ar−H), 7.28 (2H, d, J = 8 Hz, Ar−H), 7.12 (1H, d, J = 8 Hz, Ar−H), 3.85 (3H, s, O−CH_3), 2.66 (3H, s, −CH_3), 2.47 (3H, s, S-CH_3). ^{13}C NMR (DMSO-d_6, 125 MHz) δ ppm: 166.5, 160.2, 160.1, 156.2, 136.5, 134.1, 133.4, 131.1, 127.3 (2C), 126.7, 121.5 (2C), 119.2, 117.5, 111.3, 55.8, 17.6, 15.8.

*2-(3-Methoxyphenyl)-4-methyl-N-phenylthiazole-5-carboxamide (**2f**).* A coarse beige powder product with R_f = 0.62 (DCM/EtOAc 1:1). The percentage yield is 57.1%. HRMS (m/z): $[M + H]^+$ calcd for $C_{18}H_{16}N_2O_2S$, 325.0555, found 325.0545.^{1}H NMR (DMSO-d_6, 500 MHz) δ ppm: 10.26 (1H, s, N−H), 7.70 (2H, d, J = 8 Hz, Ar−H), 7.55 (1H, d, J = 7.5 Hz, Ar−H), 7.50−7.44 (2H, m, Ar−H), 7.37 (2H, t, J = 7.5 Hz, Ar−H), 7.15−7.11 (2H, m, Ar−H), 3.86 (3H, s, O−CH_3), 2.66 (3H, s, −CH_3). ^{13}C NMR (DMSO-d_6, 125 MHz) δ ppm: 166.5, 160.3, 160.2, 156.1, 139.1, 134.1, 131.1, 129.1 (2C), 126.8, 124.5, 120.8 (2C), 119.3, 117.5, 111.3, 55.8, 17.6.

*N-(2,4-Dimethoxyphenyl)-2-(4-methoxyphenyl)-4-methylthiazole-5-carboxamide (**2g**).* A soft green powder product with R_f: 0.72 (DCM/EtOAc 1:1). The percentage yield is 61%. HRMS (m/z): $[M + H]^+$ calcd for $C_{20}H_{20}N_2O_4S$, 385.1085, found 385.1178 ^{1}H NMR (DMSO-d_6, 500 MHz) δ ppm: 9.22 (1H, s, N−H), 7.56 (1H, d, J = 8 Hz, Ar−H), 7.53 (1H, d, J = 7.5 Hz, Ar−H), 7.48−7.43 (2H, m, Ar−H), 7.11 (1H, d, J = 8 Hz, Ar−H), 6.68 (1H, s, Ar−H), 6.55 (1H, d, J = 8.5 Hz, Ar−H), 3.85, 3.83, 3.78 (9H, s, O−CH_3), 2.69 (3H, s, −CH_3). ^{13}C NMR (DMSO-d_6, 125 MHz) δ ppm: 166.5, 160.3, 160.2, 158.4, 155.4, 153.4, 134.2, 131.0, 125.9, 119.9, 119.3, 117.4, 111.3, 104.7, 99.4, 97.3, 56.3, 55.8, 55.8, 17.6.

*N-(2,5-Dimethoxyphenyl)-2-(3-methoxyphenyl)-4-methylthiazole-5-carboxamide (**2h**).* A soft gray powder product with R_f = 0.50 (DCM/EtOAc 1:1). The percentage yield is 40%. HRMS (m/z): $[M + H]^+$ calcd for $C_{20}H_{20}N_2O_4S$, 385.1085, found 385.1205. ^{1}H NMR (DMSO-d_6, 500 MHz) δ ppm: 9.21 (1H, s, N−H), 7.60 (1H, s, Ar−H), 7.55 (1H, d, J = 7.5 Hz, Ar−H), 7.49−7.44 (2H, m, Ar−H), 7.12 (1H, d, J = 8.5 Hz, Ar−H), 7.04 (1H, d, J = 9 Hz, Ar−H), 6.75 (1H, d, J = 9 Hz, Ar−H), 3.86, 3.83, 3.73 (9H, s, O−CH_3), 2.72 (3H, s, −CH_3). ^{13}C NMR (DMSO-d_6, 125 MHz) δ ppm: 166.9, 160.2, 159.9, 155.5, 153.4, 145.1, 134.1, 131.1, 127.8, 127.8, 119.3, 117.5, 112.6, 111.4, 110.0, 109.6, 56.9, 55.9, 55.8, 17.7.

*N-(4-(2-Methoxyphenoxy)phenyl)-2-(3-methoxyphenyl)-4-methylthiazole-5-carboxamide (**2i**).* A soft white powder product with R_f = 0.78 (DCM/EtOAc 1:1). The percentage yield is 65.2%. HRMS (m/z): $[M + H]^+$ calcd for $C_{25}H_{22}N_2O_4S$, 447.1390, found 447.1373. ^{1}H NMR (DMSO-d_6, 500 MHz) δ ppm: 10.20 (1H, s, N−H), 7.62 (2H, d, J = 8 Hz, Ar−H), 7.55 (1H, d, J = 7.5 Hz, Ar−H), 7.49−7.44 (2H, m, Ar−H), 7.21−7.16 (2H, m, Ar−H), 7.12 (1H, d, J = 8 Hz, Ar−H), 7.03 (1H, d, J = 8 Hz, Ar−H), 6.99 (1H, t, J = 7 Hz, Ar−H), 6.86 (2H, d, J = 8 Hz, Ar−H), 3.85, 3.76 (6H, s, O−CH_3), 2.65 (3H, s, −CH_3). ^{13}C NMR (DMSO-d_6, 125 MHz) δ ppm: 166.4, 160.2, 160.0, 156.0, 154.6, 151.7, 144.4, 134.1, 133.6, 131.1, 126.7, 125.8, 122.6, 121.7, 121.5, 119.2, 117.4, 116.9 (2C), 113.9 (2C), 111.3, 56.1, 55.8, 17.6.

*2-(3-Methoxyphenyl)-4-methyl-N-(3-(trifluoromethyl)phenyl)thiazole-5-carboxamide (**2j**).* A coarse white powder product with R_f = 0.65 (DCM/EtOAc 1:1). The percentage yield is 86.3%. HRMS (m/z): $[M + H]^+$ calcd for $C_{19}H_{15}F_3N_2O_2S$, 393.0780, found 393.0772. ^{1}H NMR (DMSO-d_6, 500 MHz) δ ppm: 10.56 (1H, s, N−H), 8.17 (1H, s, Ar−H), 7.96 (1H, d, J = 8 Hz, Ar−H), 7.62 (1H, d, J = 7.5 Hz, Ar−H), 7.56 (1H, d, J = 7.5 Hz, Ar−H), 7.50−7.45 (3H, m, Ar−H), 7.13 (1H, d, J = 7.5 Hz, Ar−H), 3.86 (3H, s, O−CH_3), 2.68 (3H, s, −CH_3). ^{13}C NMR (DMSO-d$_6$, 125 MHz) δ ppm: 166.9, 160.6, 160.3, 157.1, 139.9, 134.0, 131.1, 130.4, 130.0, 129.8, 125.9, 124.4, 120.8, 119.3, 117.6, 116.9, 111.4, 55.8, 17.7.

Biological Methods. *Biological COX Assay Method.* The inhibitory impact of arachidonic acid PGH2 conversion by human recombinant COX-2 and bovine COX-1 was estimated using the COX (human) Inhibitor Screening Test Kit (provided by Cayman chemicals assay kit No. 560131). The synthesized product has a similar structure to celecoxib, so as a positive control in the test, celecoxib was employed. The testing method and reagents were prepared as the manufacturer recommended. Various concentrations of the compounds and celecoxib were dissolved in dimethylsulfoxide (DMSO) and then incubated for 10 min at 37 °C with a mixture of COX-1 or COX-2 enzymes. The reaction was initiated by adding 10 μL of arachidonic acid and incubating for 30 s at 37 °C. 30 μL of stannous chloride was added to stop the enzyme catalysis, followed by incubation for 5 min at room temperature. Quantification by ELISA was performed on produced prostaglandins. On an orbital shaker, a 96-well plate was wrapped in a plastic film and then incubated for 18 h at room temperature. After that, the plate was washed five times by using a wash buffer after emptying the wells; then, 200 μL of Ellman's reagent was added to each well and 5 μL of the tracer to the TA wells. The plate was incubated in a dark place for 60−90 min at room temperature until the absorbance of B0 and in the 0.3−0.8 range at 405 nm. A Unilab microplate reader 6000 was used for reading the plate. IC_{50} was calculated from the curve of the inhibitory response to concentration. To calculate the selectivity index (SI), the IC_{50} COX-1 and COX-2 were divided.[37]

Cell Culture and MTS assay. Breast carcinoma (MCF-7), melanoma (B16F1), hepatocellular carcinoma (HepG2 and Hep3B), cervical adenocarcinoma (HeLa), colon adenocarcinoma (Colo205), and colorectal adenocarcinoma (Caco-2), as well as the normal cell line (Hek293T), were used as cancer and normal cell lines and were grown in RPMI 1640 media with 1% penicillin/streptomycin antibiotics, 10% fetal bovine serum, and 1% L-glutamine. In general, the culture media were carefully perfused from the culture vessel without causing cell monolayer defect, and the culture flask was gently tilted. DPBS was aspirated from the culture flask without causing a defect on

https://doi.org/10.1021/acsomega.3c03256
ACS Omega 2023, 8, 29512−29526

the cell monolayer, and 1 mL of Trypsin was added, gently tilted, and incubated at 37 °C for 5 min. When the majority of cells were separated, 10 mL of corresponding culture media were added, and the culture suspension was gently vortexed or pipetted to guarantee the neutralization was complete. The cells were gently pipetted up and down 4−6 times till reaching a similar distribution, and then 10 μL of the cell suspension was added between the hemocytometer and cover glass. The number of cells needed in all four outer squares was counted, 1×10^4 cell/mL (1×10^3 cell/100 μL), and 100 μL/well was added (96-well plate was used) and then incubated at 37 °C for 24 h. Then, the media were removed carefully to avoid disturbing the cell. With the addition of 100 μL/well of different drug concentrations (300, 100, 50, and 10 μM), which was prepared before and then incubated for 72 h at 37 °C, the drug was removed without causing a disturbance in the cell to stop the effect of the drug on absorbance, following the manufacturer's recommendations. The CellTilter 96 aqueous one solution cell proliferation (MTS) test evaluated the viability of the cells (Promega Corporation, Madison, WI). 20 μL of MTS solution was added and incubated for 2 h, and then the absorbance was read by an ELISA reader at 49 nm and IC_{50} was calculated.[38]

Virtual Screening Analysis. *Molecular Docking Studies.* Out of the 10 newly designed molecules, ligands A, B, and J, which displayed the most potency and highest selectivity index (SI) values toward the COX-2 isoform, were selected for docking studies. Starting with building the 3D structures and preparing the selected ligands to be convenient for docking studies, the build panel integrated into Maestro-Schrödinger 12.1 was utilized, followed by subjecting to the Ligprep module for preparation, which involves realistic bond angles and bond length, the addition of hydrogens, generation of ionization states at the target pH (7.0 ± 2.0) protonation state, stereo chemistries and ring conformations, tautomers, low-energy structures, and corrected chiralities. Then, the generated geometries of prepared ligands were minimized at the optimized potential for the liquid simulation (OPLS-2005) force field using a default setting until getting an RMSD cut of 0.001 Å. The final minimized structures were then saved for docking studies.

Both crystallized human cyclooxygenase enzymes COX-1 (PDB ID: 3KK6) and COX-2 (PDB ID: 5KIR) complexed with celecoxib and rofecoxib, respectively, were downloaded from the Protein Data Bank.[39] These two crystal structures were evaluated properly in previous studies and displayed relevant binding orientations.[6] By use of the Protein Preparation Wizard already incorporated in the Maestro program, the obtained PDB complex structures were optimized chemically and structurally.[40] Also, the protein preparation tool aims to add H-atoms to the receptor structures, remove water molecules beyond 5 Å from the hit group, and assign bonding orders and charges. Then, the prepared protein structures were reduced using the OPLS_2005 force field with a root mean square deviation (RMSD) value of 0.30 Å. To define the active site docking studies, the Maestro Receptor Grid Generation tool was used to create the receptor grids, and the default parameters were kept. At last, to conduct molecular docking experiments, the finally prepared ligands and generated receptor grids were exported to the Glide module integrated into Maestro-Schrödinger molecular modeling software, and the extra-precision Glide docking mode was employed.[41,42] The docked position with the lowest docking score (Glide score) out of all those created for each ligand was kept as the best pose and saved for each ligand. To precisely investigate the binding interactions within the binding pocket, ultimately chosen docked postures were exported to the Protein−Ligand Interaction Profiler (PLIP) server and visualized using PyMol 2.5.2 software.[43,44]

Free Energy Calculations Using Prime MM-GBSA. To evaluate the ligand strain energies and the ligand binding energies regarding the selected docked molecules inside the location where COX-1 and COX-2 receptors bind, the Prime Molecular Mechanics Generalized Born Model and Solvent accessibility (Prime MM-GBSA) model was used, which is integrated into the Maestro-Schrödinger 12.1 program. The Prime MM-GBSA model worked at the VSGB solvent model and the OPLS-2005 force field.[45] Thus, the total free energy of ligand−receptor binding was calculated using the resulting viewer file for the docked ligands' glide positions. Upon binding, the following equation is applied to calculate the changes in free energy

$$\Delta G_{bind} = G_{complex} - (G_{protein} + G_{ligand}) \quad (1)$$

where ΔG_{bind} is the ligand binding energy, and $G_{complex}$, $G_{protein}$, and G_{ligand} are, respectively, the minimized energies of the protein−ligand complex, the unbound protein, and the unbound ligand.

Density Functional Theory Analysis. The obtained conformations of selected ligands (A, B, and J) and celecoxib were exported to the Jaguar module (Schrödinger) to perform DFT calculations. Subsequently, a group of global reactivity descriptors could be defined as the lowest unoccupied molecular orbital (E_{LUMO}), highest occupied molecular orbital (E_{HOMO}), HOMO−LUMO gap (ΔE), and atomic electrostatic potential (ESP) charges.[46,47] Using DFT, the geometries of selected ligands were properly optimized involving the use of the basis set of 6-31G** and the Becke three-parameter exchange potential and the Yang−Parr correlation functional (B3LYP).[48−50]

The HOMO orbital with elevated energy values is always directly related to an electrophilic attack due to the strong ability to donate electrons. Otherwise, the high probability of LUMO orbitals accepting electrons makes its straightforward correlation with a nucleophilic attack.[51,52] The distinction in energies between HOMO and LUMO is the electronic excitation energy named the HOMO−LUMO gap (ΔE) energy, which is a descriptor applied to assess the molecular reactivity and stability.[53,54] By decreasing the ΔE value, the molecule's global hardness decreases, indicating the molecule's high reactivity but concomitantly, with low stability.[55]

The electrostatic potential map surfaces of the selected ligand were also constituted using DFT calculations within the Jaguar module to specify the electron-rich regions and electron-poor concentrate regions.

Drug-Likeness Analysis. The drug-likeness of all our recently developed compounds was evaluated by calculating a set of descriptors related to ADME-T. This set of ADME-T parameters was determined to ensure that the newly designed ligands agreed with the potential drug candidates concerning physicochemical and pharmacokinetic parameters. The ADME-T descriptors were determined utilizing the QikProp module of the Schrödinger suite (Schrödinger Release 2021-4). It is easy to use, quick, and accurate.[56]

https://doi.org/10.1021/acsomega.3c03256
ACS Omega 2023, 8, 29512−29526

Statistical Analyses. The biological activities were determined in triplicate for each sample. The results were provided as means of the standard deviation (±SD).

■ ASSOCIATED CONTENT

Supporting Information

The Supporting Information is available free of charge at https://pubs.acs.org/doi/10.1021/acsomega.3c03256.

Figures S1−S10 contain the IUPAC names; chemical structures; and NMR spectra of all compounds (PDF)

■ AUTHOR INFORMATION

Corresponding Authors

Mohammed Hawash − *Department of Pharmacy, Faculty of Medicine and Health Sciences, An-Najah National University, Nablus 400, Palestine;* orcid.org/0000-0001-5640-9700; Phone: +972569939939; Email: mohawash@najah.edu

Nidal Jaradat − *Department of Pharmacy, Faculty of Medicine and Health Sciences, An-Najah National University, Nablus 400, Palestine;* orcid.org/0000-0003-2291-6821; Phone: +972 59-973-9476; Email: nidaljaradat@najah.edu

Authors

Rozan Sabobeh − *Department of Pharmacy, Faculty of Medicine and Health Sciences, An-Najah National University, Nablus 400, Palestine*

Murad Abualhasan − *Department of Pharmacy, Faculty of Medicine and Health Sciences, An-Najah National University, Nablus 400, Palestine*

Mohammed T. Qaoud − *Department of Pharmaceutical Chemistry, Faculty of Pharmacy, Gazi University, 06330 Ankara, Turkey*

Complete contact information is available at: https://pubs.acs.org/10.1021/acsomega.3c03256

Notes

The authors declare no competing financial interest.

■ ACKNOWLEDGMENTS

The authors wish to thank An-Najah National University and Gazi University for their support in carrying out this work. The authors would like to thank the Faculty of Graduate Studies at An-Najah National University for facilitating the achievement of this work. There was no fund received for this research.

■ REFERENCES

(1) Zarghi, A.; Arfaei, S. Selective COX-2 inhibitors: a review of their structure-activity relationships. *Iran. J. Pharm. Res.* **2011**, *10*, 655−683.

(2) Fiorucci, S.; Meli, R.; Bucci, M.; Cirino, G. Dual inhibitors of cyclooxygenase and 5-lipoxygenase. A new avenue in anti-inflammatory therapy? *Biochem. Pharmacol.* **2001**, *62*, 1433−1438.

(3) Hawash, M.; Jaradat, N.; Abualhasan, M.; Qneibi, M.; Rifai, H.; Saqfelhait, T.; Shqirat, Y.; Nazal, A.; Omarya, S.; Ibrahim, T.; Sobuh, S.; Zarour, A.; Mousa, A. Evaluation of cytotoxic, COX inhibitory, and antimicrobial activities of novel isoxazole-carboxamide derivatives. *Lett. Drug Des. Discovery* **2022**, *19*, No. 12.

(4) Day, R. O.; Graham, G. G.Non-steroidal anti-inflammatory drugs (NSAIDs) *BMJ* 2013, p 346.

(5) BAYTAŞ, S.; Dural, N. N. T.; ÖZKAN, Y.; ŞİMŞEK, H. B.; Gürsel, T.; Ünlü, S. Synthesis, anti-inflammatory, antiplatelet and in silico evaluations of (E)-3-(3-(2, 3-dihydro-3-methyl-2-oxo-3H-benzoxazole-6-yl)-1-phenyl-1H-pyrazole-4-yl) acrylamides. *Turk. J. Chem.* **2012**, *36*, 367−382.

(6) Assali, M.; Abualhasan, M.; Sawaftah, H.; Hawash, M.; Mousa, A. Synthesis, biological activity, and molecular modeling studies of pyrazole and triazole derivatives as selective COX-2 inhibitors. *J. Chem.* **2020**, *2020*, 1−14.

(7) Bayly, C. I.; Black, W. C.; Léger, S.; Ouimet, N.; Ouellet, M.; Percival, M. D. Structure-based design of COX-2 selectivity into flurbiprofen. *Bioorg. Med. Chem. Lett.* **1999**, *9*, 307−312.

(8) Patrick, G. L. *An Introduction to Medicinal Chemistry*; Oxford university press, 2013.

(9) Vane, J. R.; Botting, R. M. Mechanism of action of nonsteroidal anti-inflammatory drugs. *Am. J. Med.* **1998**, *104*, 2S−8S.

(10) Kumar, J. D.; Zanderigo, F.; Prabhakaran, J.; Rubin-Falcone, H.; Parsey, R. V.; Mann, J. J. In vivo evaluation of [11C] TMI, a COX-2 selective PET tracer, in baboons. *Bioorg. Med. Chem. Lett.* **2018**, *28*, 3592−3595.

(11) Hermann, M.; Ruschitzka, F. Coxibs, non-steroidal anti-inflammatory drugs and cardiovascular risk. *Intern. Med. J.* **2006**, *36*, 308−319.

(12) Zarghi, A.; Ghodsi, R. Design, synthesis, and biological evaluation of ketoprofen analogs as potent cyclooxygenase-2 inhibitors. *Bioorg. Med. Chem.* **2010**, *18*, 5855−5860.

(13) Hawash, M.; Jaradat, N.; Abualhasan, M.; Qaoud, M. T.; Joudeh, Y.; Jaber, Z.; Sawalmeh, M.; Zarour, A.; Mousa, A.; Arar, M. Molecular docking studies and biological evaluation of isoxazole-carboxamide derivatives as COX inhibitors and antimicrobial agents. *3 Biotech* **2022**, *12*, 1−16.

(14) Liaras, K.; Fesatidou, M.; Geronikaki, A. Thiazoles and thiazolidinones as COX/LOX inhibitors. *Molecules* **2018**, *23*, 685.

(15) Sharma, R. N.; Xavier, F. P.; Vasu, K. K.; Chaturvedi, S. C.; Pancholi, S. S. Synthesis of 4-benzyl-1, 3-thiazole derivatives as potential anti-inflammatory agents: an analogue-based drug design approach. *J. Enzyme Inhib. Med. Chem.* **2009**, *24*, 890−897.

(16) El-Achkar, G. A.; Jouni, M.; Mrad, M. F.; Hirz, T.; El Hachem, N.; Khalaf, A.; Hammoud, S.; Fayyad-Kazan, H.; Eid, A. A.; Badran, B.; et al. Thiazole derivatives as inhibitors of cyclooxygenases in vitro and in vivo. *Eur. J. Pharmacol.* **2015**, *750*, 66−73.

(17) Oniga, S. D.; Pacureanu, L.; Stoica, C. I.; Palage, M. D.; Crăciun, A.; Rusu, L. R.; Crisan, E.-L.; Araniciu, C. COX inhibition profile and molecular docking studies of some 2-(trimethoxyphenyl)-thiazoles. *Molecules* **2017**, *22*, 1507.

(18) Hawash, M.; Jaradat, N.; Abualhasan, M.; Şüküroğlu, M. K.; Qaoud, M. T.; Kahraman, D. C.; Daraghmeh, H.; Maslamani, L.; Sawafta, M.; Ratrout, A.; Issa, L. Design, synthesis, molecular docking studies and biological evaluation of thiazole carboxamide derivatives as COX inhibitors. *BMC Chem.* **2023**, *17*, 11.

(19) Koki, A. T.; Masferrer, J. L. Celecoxib: a specific COX-2 inhibitor with anticancer properties. *Cancer Control* **2002**, *9*, 28−35.

(20) Kundu, N.; Fulton, A. M. Selective cyclooxygenase (COX)-1 or COX-2 inhibitors control metastatic disease in a murine model of breast cancer. *Cancer Res.* **2002**, *62*, 2343−2346.

(21) Veltman, J. D.; Lambers, M. E.; van Nimwegen, M.; Hendriks, R. W.; Hoogsteden, H. C.; Aerts, J. G.; Hegmans, J. P. COX-2 inhibition improves immunotherapy and is associated with decreased numbers of myeloid-derived suppressor cells in mesothelioma. Celecoxib influences MDSC function. *BMC Cancer* **2010**, *10*, 1−13.

(22) Gerbino, P. P. Emerging evidence in NSAID pharmacology: important considerations for product selection. *Am. J. Manage. Care* **2015**, *21*, S139−S147.

(23) Hawash, M.; Kahraman, D. C.; Ergun, S. G.; Cetin-Atalay, R.; Baytas, S. N. Synthesis of novel indole-isoxazole hybrids and evaluation of their cytotoxic activities on hepatocellular carcinoma cell lines. *BMC Chem,* **2021**, *15*, No. 66.

(24) Huo, X.-S.; Jian, X.-E.; Ou-Yang, J.; Chen, L.; Yang, F.; Lv, D.-X.; You, W.-W.; Rao, J.-J.; Zhao, P.-L. Discovery of highly potent tubulin polymerization inhibitors: Design, synthesis, and structure-activity relationships of novel 2, 7-diaryl-[1, 2, 4] triazolo [1, 5-a] pyrimidines. *Eur. J. Med. Chem.* **2021**, *220*, No. 113449.

(25) Sun, Y.-X.; Song, J.; Kong, L.-J.; Sha, B.-B.; Tian, X.-Y.; Liu, X.-J.; Hu, T.; Chen, P.; Zhang, S.-Y. Design, synthesis and evaluation of novel bis-substituted aromatic amide dithiocarbamate derivatives as colchicine site tubulin polymerization inhibitors with potent anticancer activities. *Eur. J. Med. Chem.* **2022**, *229*, No. 114069.
(26) Song, J.; Wang, S.-H.; Song, C.-H.; Zhang, W.-X.; Zhu, J.-X.; Tian, X.-Y.; Fu, X.-J.; Xu, Y.; Jin, C.-Y.; Zhang, S.-Y. Discovery of N-benzylarylamide derivatives as novel tubulin polymerization inhibitors capable of activating the Hippo pathway. *Eur. J. Med. Chem.* **2022**, *240*, No. 114583.
(27) Mohamed, H. S.; Amin, N. H.; El-Saadi, M. T.; Abdel-Rahman, H. M. Design, synthesis, biological assessment, and in-Silico studies of 1, 2, 4-triazolo [1, 5-a] pyrimidine derivatives as tubulin polymerization inhibitors. *Bioorg. Chem.* **2022**, *121*, No. 105687.
(28) Hawash, M. Recent Advances of Tubulin Inhibitors Targeting the Colchicine Binding Site for Cancer Therapy. *Biomolecules* **2022**, *12*, 1843.
(29) Crisan, L.; Borota, A.; Bora, A.; Pacureanu, L. Diarylthiazole and diarylimidazole selective COX-1 inhibitor analysis through pharmacophore modeling, virtual screening, and DFT-based approaches. *Struct. Chem.* **2019**, *30*, 2311−2326.
(30) Asiri, A. M.; Karabacak, M.; Kurt, M.; Alamry, K. A. Synthesis, molecular conformation, vibrational and electronic transition, isometric chemical shift, polarizability and hyperpolarizability analysis of 3-(4-Methoxy-phenyl)-2-(4-nitro-phenyl)-acrylonitrile: a combined experimental and theoretical analysis. *Spectrochim. Acta, Part A* **2011**, *82*, 444−455.
(31) Kosar, B.; Albayrak, C. Spectroscopic investigations and quantum chemical computational study of (E)-4-methoxy-2-[(p-tolylimino) methyl] phenol. *Spectrochim. Acta, Part A* **2011**, *78*, 160−167.
(32) Parr, R. G.; Chattaraj, P. K. Principle of maximum hardness. *J. Am. Chem. Soc.* **1991**, *113*, 1854−1855.
(33) Kenny, P. W. Hydrogen bonding, electrostatic potential, and molecular design. *J. Chem. Inf. Model.* **2009**, *49*, 1234−1244.
(34) Eid, A. M.; Hawash, M.; Amer, J.; Jarrar, A.; Qadri, S.; Alnimer, I.; Sharaf, A.; Zalmoot, R.; Hammoudie, O.; Hameedi, S.; Mousa, A. Synthesis and biological evaluation of novel isoxazole-amide analogues as anticancer and antioxidant agents. *BioMed Res. Int.* **2021**, *2021*, 1−9.
(35) Hawash, M.; Jaradat, N.; Abualhasan, M.; Amer, J.; Levent, S.; Issa, S.; Ibrahim, S.; Ayaseh, A.; Shtayeh, T.; Mousa, A. Synthesis, chemo-informatics, and anticancer evaluation of fluorophenyl-isoxazole derivatives. *Open Chem.* **2021**, *19*, 855−863.
(36) Hawash, M.; Jaradat, N.; Bawwab, N.; Salem, K.; Arafat, H.; Hajyousef, Y.; Shtayeh, T.; Sobuh, S. Design, synthesis, and biological evaluation of phenyl-isoxazole-carboxamide derivatives as anticancer agents. *Heterocyclic Communications* **2021**, *27*, 133−141.
(37) Drazen, J. M. COX-2 inhibitors–a lesson in unexpected problems. *N. Engl. J. Med.* **2005**, *352*, 1131−1132.
(38) Hawash, M.; Qaoud, M. T.; Jaradat, N.; Abdallah, S.; Issa, S.; Adnan, N.; Hoshya, M.; Sobuh, S.; Hawash, Z. Anticancer Activity of Thiophene Carboxamide Derivatives as CA-4 Biomimetics: Synthesis, Biological Potency, 3D Spheroid Model, and Molecular Dynamics Simulation. *Biomimetics* **2022**, *7*, 247.
(39) Berman, H. M.; Westbrook, J.; Feng, Z.; Gilliland, G.; Bhat, T. N.; Weissig, H.; Shindyalov, I. N.; Bourne, P. E. The protein data bank. *Nucleic Acids Res.* **2000**, *28*, 235−242.
(40) Impact, S. LLC, New York, NY; Prime, Schrödinger, LLC, New York, NY, Google Scholar There is no corresponding record for this reference. 2021.
(41) Friesner, R. A.; Banks, J. L.; Murphy, R. B.; Halgren, T. A.; Klicic, J. J.; Mainz, D. T.; Repasky, M. P.; Knoll, E. H.; Shelley, M.; Perry, J. K. Glide: a new approach for rapid, accurate docking and scoring. 1. Method and assessment of docking accuracy. *J. Med. Chem.* **2004**, *47*, 1739−1749.
(42) Halgren, T. A.; Murphy, R. B.; Friesner, R. A.; Beard, H. S.; Frye, L. L.; Pollard, W. T.; Banks, J. L. Glide: a new approach for rapid, accurate docking and scoring. 2. Enrichment factors in database screening. *J. Med. Chem.* **2004**, *47*, 1750−1759.
(43) Adasme, M. F.; Linnemann, K. L.; Bolz, S. N.; Kaiser, F.; Salentin, S.; Haupt, V. J.; Schroeder, M. PLIP 2021: expanding the scope of the protein−ligand interaction profiler to DNA and RNA. *Nucleic Acids Res.* **2021**, *49*, W530−W534.
(44) Schrödinger, L. *The PyMOL Molecular Graphics System*, version 1.3 r1. August, 2010.
(45) Li, J.; Abel, R.; Zhu, K.; Cao, Y.; Zhao, S.; Friesner, R. A. The VSGB 2.0 model: a next generation energy model for high resolution protein structure modeling. *Proteins: Struct., Funct., Bioinf.* **2011**, *79*, 2794−2812.
(46) Jaguar, V. *9.1 Schrödinger Suite Release 2016-1*; Schrödinger, LLC: New York, NY, USA, 2016.
(47) Bochevarov, A. D.; Harder, E.; Hughes, T. F.; Greenwood, J. R.; Braden, D. A.; Philipp, D. M.; Rinaldo, D.; Halls, M. D.; Zhang, J.; Friesner, R. A. Jaguar: A high-performance quantum chemistry software program with strengths in life and materials sciences. *Int. J. Quantum Chem.* **2013**, *113*, 2110−2142.
(48) Gill, P. M.; Johnson, B. G.; Pople, J. A.; Frisch, M. J. The performance of the Becke—Lee—Yang—Parr (B—LYP) density functional theory with various basis sets. *Chem. Phys. Lett.* **1992**, *197*, 499−505.
(49) Lee, C.; Yang, W.; Parr, R. G. Development of the Colle-Salvetti correlation-energy formula into a functional of the electron density. *Phys. Rev. B: Condens. Matter Mater. Phys.* **1988**, *37*, 785.
(50) Stephens, P. J.; Devlin, F. J.; Chabalowski, C. F.; Frisch, M. J. Ab initio calculation of vibrational absorption and circular dichroism spectra using density functional force fields. *J. Phys. Chem. A* **1994**, *98*, 11623−11627.
(51) Nassabeh, N.; Tran, M.; Fleming, P. E. Dissociation of the ethyl radical: an exercise in computational chemistry. *J. Chem. Educ.* **2014**, *91*, 1248−1253.
(52) Clare, B. W. Charge transfer complexes and frontier orbital energies in QSAR: a congeneric series of electron acceptors. *THEOCHEM* **1995**, *337*, 139−150.
(53) Zhan, C.-G.; Nichols, J. A.; Dixon, D. A. Ionization potential, electron affinity, electronegativity, hardness, and electron excitation energy: molecular properties from density functional theory orbital energies. *J. Phys. Chem. A* **2003**, *107*, 4184−4195.
(54) Zheng, Y.; Zheng, M.; Ling, X.; Liu, Y.; Xue, Y.; An, L.; Gu, N.; Jin, M. Design, synthesis, quantum chemical studies and biological activity evaluation of pyrazole−benzimidazole derivatives as potent Aurora A/B kinase inhibitors. *Bioorg. Med. Chem. Lett.* **2013**, *23*, 3523−3530.
(55) Zhou, Z.; Parr, R. G. Activation hardness: new index for describing the orientation of electrophilic aromatic substitution. *J. Am. Chem. Soc.* **1990**, *112*, 5720−5724.
(56) Elekofehinti, O. O.; Iwaloye, O.; Famusiwa, C. D.; Akinseye, O.; Rocha, J. B. Identification of main protease of coronavirus SARS-CoV-2 (Mpro) Inhibitors from Melissa officinalis. *Curr. Drug Discovery Technol.* **2021**, *18*, 38−52.

https://doi.org/10.1021/acsomega.3c03256
ACS Omega 2023, 8, 29512−29526